Antifreeze-infused superhydrophobic surface with superb anti-icing and anti-frosting performance

Wei Weng[1,*], *Yueying Yu*[1,2], *Masanobu Naito*[1,2,*]

[1]Research Center for Macromolecules and Biomaterials, National Institute for Materials Science (NIMS), 1-2-1 Sengen, Tsukuba, Ibaraki, 305-0047, Japan

[2]Graduate School of Science and Technology, University of Tsukuba, 1-1-1 Tennodai, Tsukuba, Ibaraki, 305-8577, Japan

[*]Corresponding authors: weng.wei@nims.go.jp, naito.masanobu@nims.go.jp

Keywords: Liquid-infused surface, superhydrophobic, antifreeze, anti-frosting, anti-icing

Abstract: As an attempt of combining antifreeze and superhydrophobicity, propylene glycol (PG) is encaged in a porous superhydrophobic skeleton composed of ZnO tetrapods and polydimethylsiloxane. At room temperature, the PG-infused skeleton presents large contact angle, small sliding angle and good repellency against impacting water drops, while it effectively defers frost emerging and growth in humid and cooling conditions. The PG-infused skeleton delays the frost onset 6 times and 18 times longer than the superhydrophobic skeleton and silicone oil-infused skeleton, respectively. Moreover, it can repeatedly serve as a frost-deterrent surface up to 10 times without replenishment, and is durable under frosting/defrosting cycles. The merits are ascribed to the non-affinity between glycol and the skeleton, and humidity sink effect and self-secretion of glycol out of the skeleton under cooling. The former lets the surface asperities of the skeleton exposed. And the latter imparts good anti-icing, anti-

frosting, and de-icing performance to the PG-infused skeleton. The work provides insights into liquid-infused surfaces and icephobic surfaces.

Introduction

Icing, or frosting, is nasty for transportation, power, and agriculture industry. Superhydrophobic surfaces constructed by low-surface-energy materials and delicate surface textures exhibit prolonged freezing delay time of sessile water drops and good repellency against impinging drops owing to the embedded air pockets.[1,2] In a humid environment, in case of condensation occurrence, anti-icing equals to anti-frosting. Water vapor preferentially nucleates in textures and expels the air pockets, which turns superhydrophobic surfaces ice-affinity.[3–5] Nonetheless, anti-frosting has been improved, though limitedly, by devising distinctive topographies enabling jumping-removal, frost-toward sliding, fast coalescence, etc.[6–9] Slippery lubricant-infused porous surfaces (SLIPS) exploit an oil layer instead of the air layer in superhydrophobic surfaces. Water drops can effortlessly slide off from SLIPS before or even after freezing.[10–12] However, condensation could be accelerated on SLIPS, which leads to severe lubricant depletion and fast frost growth.[13,14]

Practically, antifreezes, e.g., salts and glycols, have been widely applied and demonstrated to be effective for anti-frosting.[15–19] Propylene glycol (PG) is a colorless, viscous liquid at room temperature, which can lower the freezing point of water to about – 60 ºC (eutectic temperature). Moreover, since it is essentially nontoxic, it has become the mainstream aviation deicing and anti-icing fluid. However, large amounts are required, e.g., ~138 kg or 600-7800 kg of PG needs to be sprayed on a Boeing 727 airplane before or after ice forms.[17] Consequently, it brings about high costs and environmental concerns because glycols may deplete dissolved oxygen in streams or lakes as they biodegrade.[20]

Fortunately, it is not necessary to form a film of antifreezes to resist frosting. Antifreeze drop arrays have been revealed to be better than a film of same amount, which delayed complete frosting over the samples 1.6 to 2.8 times longer than the films.[21] Moreover, many antifreeze-imbibed hydrophilic surfaces have been developed, possessing several merits including better anti-frosting performance than the matrix hydrophilic surfaces, low antifreeze amount, and broad applications.[17,18,22–24] However, they should be replenished every time after using and lose antifreezes quickly when being contacted with water/running water. To this end, bilayer structure was proposed, in which the bottom antifreeze-imbibed hydrophilic layer is protected by the top hydrophobic or superhydrophobic layer.[16,25,26] Not only can the bilayer surfaces contact with water but also their anti-frosting ability is better than the ones without protective layers. However, the durability is not good enough because antifreeze-imbibed hydrophilic layers absorb water vapor from the humid environment, swell, and expand during freezing, resulting in large stress at interfaces.

Herein, an antifreeze-infused superhydrophobic surface is facilely prepared by sucking PG into a porous superhydrophobic skeleton, maintaining PG's excellent anti-icing/anti-frosting property and skeleton's superhydrophobicity, and not having bilayer structure's durability problem. Briefly, the developed surface has a contact angle of > 160º and a sliding angle of < 10º, also is able to repel impacting water drops. And no frost is formed up to 180 min at -10 ºC, and to 60 min at -30 ºC. Moreover, the surface can be repeatedly used for anti-frosting at -10 ºC up to 10 times without replenishment. And the surface is intact after 20 cycles of frosting/defrosting at -30 ºC.

Materials and methods

Materials

Polydimethylsiloxane (PDMS, HC2100) was purchased from Toray Industries, Inc. (Japan). Ethyl acetate (EtOAc, 99.5%), ethylene glycol (EG), and PG were from Wako Pure Chemical Industries (Japan). Silicone oil (KF-96-100cs) and ZnO tetrapods (WZ-0501) were bought from Shin-Etsu Chemical Co., Ltd. (Japan) and AMTEC Co., Ltd. (Japan), respectively. Glass slides with sizes of 26 mm × 76 mm × 1.2~1.5 mm (S7224, Matsunami Glass Ind., Ltd., Japan) were used as coating substrates.

Preparation of superhydrophobic skeletons

6 g PDMS was dissolved in 300 ml EtOAc. Afterwards, 54 g ZnO tetrapods were added to form a suspension. After having been stirred overnight, the suspension with an amount of 1 mL was drop-coated on glass slides, which were plasma-treated beforehand. Finally, superhydrophobic skeletons were obtained after heat-treatment in 120 ºC for 2 h. Actually, different weight ratios of ZnO to PDMS, such as 9:1, 7:3, 5:5 and 3:7, were tried while weight concentrations of ZnO and PDMS in EtOAc were fixed.

Liquid infusion

Superhydrophobic skeletons immersed into PG or silicone oil bath were put inside a vacuum chamber (VOS-310C, EYELA, Japan). Then, the chamber pressure was gradually decreased and reached a vacuum of 0.102 MPa, at which air entrapped in the superhydrophobic skeletons were removed and instead PG or silicone oil was infused into the voids of skeletons. Finally, the liquid-infused skeletons were spun at 2000 rpm for 1 min to shed the excess liquid on the surface. And PG-infused skeletons were stored at subzero temperatures, where PG has negligible vapor pressure.[17] Similarly, EG was infused into superhydrophobic skeletons using same procedures.

Morphology and wettability characterization

Superhydrophobic skeletons, PG-infused skeletons, and oil-infused skeletons were characterized by field emission scanning electron microscope (FESEM, JSM-7001F, JEOL, Japan), scanning electron microscope (SEM, Miniscope TM4000, Hitachi, Japan), laser confocal scanning microscope (Optelics HYBRID C3, Lasertec, Japan), and atomic force microscope (AFM, NanoWizard 4 XP, Bruker, USA). Compositions of water, PG, PG-infused skeletons, and condensed drops on PG-infused skeletons during frosting test were detected by Raman microscope (inVia Reflex, Renishaw, UK). Laser of 532 nm and grating of 1800 l mm^{-1} were used. Wettability including contact angles (CAs), advancing contact angles (θ_{adv}), receding contact angles (θ_{rec}), and sliding angles (SAs) were measured by DMs-401-type CA meter (Kyowa Interface Science, Japan). Water drop sliding and impacting were also recorded by a high-speed camera (Mini AX, FASTCAM, Photron, Japan). Porosity and pore size were measured for superhydrophobic skeletons by a mercury porosimeter (AutoPore IV 9520, Micromeritics-Shimadzu, Japan).

Anti-icing, de-icing, and anti-frosting test

Regarding frosting test, the temperature of samples was controlled by a cooling stage (10083L, High Tech Co., Ltd., Japan), which was set at -10 ºC or -30 ºC. Meanwhile, the ambient relative humidity and temperature were 42 ± 2% and 10 ± 1 ºC, respectively. Specifically, test samples were cooled from the ambient temperature to a target temperature at 10 ºC min^{-1} and kept at the target temperature for 10 min under N_2 atmosphere. After that, the N_2 protection was removed and the samples were exposed to the ambient conditions, from which frosting started and was monitored. For icing test, water drops of 10 μL were dripped on samples. Drops, together with samples, were cooled from the ambient temperature at 1 ºC min^{-1} under the

ambient conditions. The cooling was stopped when the drops were frozen. And the corresponding temperature was taken as ice nucleation temperature (INT). Regarding de-icing test, cuvettes were put on test samples that were placed on the cooling stage. 1 mL of water was added into the cuvettes. Water and test samples were cooled to -10 ºC and lasted for 3 h. Afterwards, digital force gauge (DST-50N, IMADA Co., Ltd.) was used to detach the cuvette-encased ice columns ($1 \times 1 \times 1$ cm^3) with a horizontal probe impact speed of 0.5 mm s^{-1}. The peak force was recorded and divided by the ice area to get the ice adhesion strength (IAS). However, the above commonly adopted test procedures could not be applied to PG-infused skeleton because water could not freeze. An alternative method was used. Ice cubes ($1 \times 1 \times 1$ cm^3) were made in a fridge at -20 ºC for 6 h, which were then transferred to the pre-cooled (-10 ºC) PG-infused skeleton. By tilting the PG-infused skeleton, the ice cubes could slide off from the surface by self-gravity.

Results and discussion

Liquid infustion into superhydrophobic skeletons

First, porosity and pore size were tested, and the results that depend on the weight percentage of ZnO in ZnO/PDMS skeletons are shown in Figure S1a and S1b. As the ZnO weight percentage increases, the porosity increases but the pore size decreases. Since larger porosity leads to more infused liquid and improved hydrophobicity according to the Cassie-Baxter equation, the ZnO weight ratio of 0.9 was selected. In other words, the superhydrophobic skeleton was composed of ZnO and PDMS with a ratio of 9:1. Its porosity is 60.9%, its average pore diameter is ~2.2 μm, and 94% of pores lie in a range of 0.5 – 10 μm. CA of PG drop on the superhydrophobic skeleton is 133.3 ± 0.6º (Figure S1c), and its θ_{adv} is 136.7 ± 0.7º, which implies that an external force is needed to infuse PG into the skeleton. The resistance force (f_r) has the following form:

$$f_r = \pi D \gamma cos\theta_{adv}, \quad (1)$$

where γ is the surface tension (0.03857 N m^{-1}) of PG, and D is the pore diameter. The exertion force (f_{ext}) has the form of

$$f_{ext} = P\pi(\frac{D}{2})^2, \quad (2)$$

where P is the vacuum pressure inside a vacuum chamber.

Here, we used P of 0.102 MPa. Then, D was derived to be 1.10 μm. Therefore, most of the pores in the skeleton could be infiltrated by PG under the vacuum treatment (Figure S1b). Regarding silicone oil, it is observed seeping into the superhydrophobic skeleton due to the capillary force (Figure S1d). Although the exertion force was not necessary for oil infusion, vacuum was still applied in order to have a same condition for both PG and oil infusion. The silicone oil infused into the skeleton has an areal mass density of 8.63 ± 0.14 mg cm^{-2}. Considering the thickness (~145 μm) of the skeleton (Figure S2), the volume occupied by oil is 61.7%, which is close to the porosity tested by a mercury porosimeter. And the areal mass density of PG is 7.48 ± 0.15 mg cm^{-2}, resulting in a PG-occupied volume of 49.8%, which means around 10% voids are free of PG. To be mentioned, 35 – 2000 mg cm^{-2} of PG is required to be sprayed onto a Boeing 727 airplane to prevent or dislodge ice,[17] which is way higher than the PG amount herein.

Surface morphology

Schematics of superhydrophobic skeleton, oil-infused skeleton, and PG-infused skeleton are shown in Figure 1a, 1b, and 1c, respectively. Due to a strong affinity between silicone oil and the skeleton, the oil covers the skeleton. On the contrary, the protrusions or the contours of the superhydrophobic skeleton expose in the air after the PG infusion. This is evidently seen from the images took by confocal laser scanning microscope (Figure 1d-1i). The superhydrophobic

skeleton becomes opaque after the oil infusion as comparing Figure 1d and 1e. Also, from 3D surface profile images (Figure 1g-1i), textures of the superhydrophobic skeleton are clearly observed and maintained after the PG infusion. Oppositely, the skeleton became smooth after the oil infusion. It is also verified from the roughness (*Sa*, arithmetic average of height difference of each point from the mean plane), which was tested to be 1.94 ± 0.07, 0.34 ± 0.01, and 1.98 ± 0.06 μm for superhydrophobic skeleton, oil-infused skeleton, and PG-infused skeleton, respectively. A top-view SEM image of the superhydrophobic skeleton is shown in Figure 1j, whose enlarged view was provided in Figure S3. And cross-sectional SEM images can be found in Figure S2. From all of them, porous structure is confirmed, which is enabled by the geometrical stacking of micro-sized ZnO tetrapods that was detailed in a previous paper.[27] Furthermore, PG-infused skeleton was probed by AFM. Height image is shown in Figure 1k, where dark parts circled by green dash lines represent the pore areas. However, something is believed to be in the pores because high adhesive forces were detected (Figure 1l), which should be the infused PG.

Surface wettability

CAs of water drops (10 μL) on superhydrophobic skeleton, oil-infused skeleton, and PG-infused skeleton were tested and the results are 161.1 ± 1.1º, 103.5 ± 0.5º, and 160.5 ± 0.7º, respectively (Figure 2a-2c). SAs of water drops (10 μL) were also measured and they are 2.7 ± 1.1º, 1.6 ± 0.5º, and 9.7 ± 2.4º accordingly. As shown in Figure 2d-2f, water drops of 10 μL are sliding off these samples. Drops are readily movable at low tilted angles on superhydrophobic skeleton and oil-infused skeleton, while a larger tilted angle is required for PG-infused skeleton. Moreover, sliding velocities are high on superhydrophobic skeleton and PG-infused skeleton. Oppositely, drop slides slowly on oil-infused skeleton because water drop needs to jostle the surrounding oil.[28]

Furthermore, water drop impacting (10 μL) was studied for superhydrophobic skeleton (Figure 2g and 2h) and PG-infused skeleton (Figure 2i and 2j). The impact velocity is 1.40 m s^{-1} for Figure 2g and 1.25 m s^{-1} for Figure 2h. When 1.40 m s^{-1} was used, water penetrated the textures, the entrapped air-pockets were lost, and partial rebounding was generated, which was indicated by the red arrow. When lowering the velocity to 1.25 m s^{-1}, water penetration was not observed, resulting in a full rebounding. There is a threshold impact velocity u_{th}, which is determined by the geometry of air-pockets (pores) as below:[29]

$$u_{th} = \sqrt{\frac{32\gamma D_p}{\rho W_p^2}}, \quad (3)$$

where γ is the surface tension of water (0.0728 N m^{-1}), ρ is the water density, D_p is the depth of pores, and W_p is the width of pores. From the surface profiles of the superhydrophobic skeleton (Figure S4), D_p of 4.01 ± 0.64 μm and W_p of 67.89 ± 18.07 μm were got, leading to u_{th} of 1.48 ± 0.24 m s^{-1}. Therefore, the experiments well agree with the theoretical predications. As for PG-infused skeleton, water penetration occurred at 0.77 m s^{-1} (Figure 2i), which disappeared at 0.63 m s^{-1} (Figure 2j). Hence, the superhydrophobicity of the ZnO/PDMS skeleton was largely maintained after PG infusion.

Anti-frosting performance

Frosting test was conducted at -10 ºC for superhydrophobic skeleton, oil-infused skeleton, and PG-infused skeleton. Before being exposed to the ambient conditions (42% of relative humidity and 10 ºC), samples were stabilized at -10 ºC for at least 10 min under N_2 protection. Time-lapsed photos under frosting are shown in Figure 3. Since all samples are white, it is difficult to check whether there is frost or not. Therefore, time-lapsed images by confocal laser scanning microscope under frosting are shown in Figure 4. Clearly, on the superhydrophobic surface formed tiny condensed drops at the very beginning of frosting (Figure 4a). And the condensed

drops grew with time, and got frozen at ~30 min. However, in Figure 3a the iced condensed drops are too small to see, and only some relatively large coalesced drops were observed after thawing. As for oil-infused skeleton, water condensation also occurred and the condensed drops were scattered on the oil film (Figure 4b). Notably, the freezing of the condensed drops was advanced to ~10 min. The reason is water condensation on the oil film was accelerated,[13] resulting in a close network of condensed drops, which then facilitated the condensation frosting.[9,30] Owing to the enhanced condensation, frosting can be seen at the sample's edges (Figure 3b), and large water-oil core-shell drops[31] are manifest after melting (Figure 4b). However, severe depletion of oil could succeed when removing these drops.

The frosting phenomenon on PG-infused skeleton is totally different from the above two cases. Several separated condensed drops occurred, grew, but did not freeze even after 180 min (Figure 3c). The area having condensed drops, such as the one circled by the red square in Figure 3c, was screened, and the results are shown in Figure 4c. No tiny condensed drops like the ones on the superhydrophobic skeleton were found. Moreover, the area not having condensed drops pointed out by the red circle in Figure 3c was also examined, and the results are shown in Figure S5, from which the area was demonstrated to be free of condensates. Hence, there are not tiny condensates but large and sparse condensed drops on PG-infused skeleton, which maintains non-frozen 6 times and 18 times longer than the condensates on superhydrophobic skeleton and oil-infused skeleton, respectively.

It has reported that antifreeze-imbibed hydrophilic/superhydrophobic bilayer surfaces have durability issue because the interfaces suffer from large stress during freezing and melting.[16,25] Here, complete frosting was induced on PG-infused skeleton at -30 ºC while the ambient conditions were same. Condensation was more severe at -30 ºC than at -10 ºC (Figure 5a). At

60 min, except the edges, the whole surface was resisting against frosting. Then, frosting propagated inwards with time. At 140 min, frost was all over the surface. Afterwards, the sample was thawed, emptied, reinfused with PG, and re-tested at -30 ºC until complete frosting over the surface. And the sample was repeated under frosting/melting/replenishing to 20 times. Seen from Figure 5b and 5c, the infused PG mass and complete frosting time are nearly unchanged in the cycle test, which demonstrates the durability of the developed PG-infused superhydrophobic skeleton. Moreover, the evolution of frost coverage at -30 ºC for superhydrophobic skeleton, oil-infused skeleton, and PG-infused skeleton is presented in Figure S6. Complete frosting on oil-infused skeleton took only 3 minutes, and superhydrophobic skeleton needed about 7 minutes. In contrast, it took at least 20 times longer for PG-infused skeleton.

To reveal the distinctiveness of PG-infused skeleton, anti-frosting of PG on hydrophilic glasses and hydrophobic PDMS films was also investigated. As seen from Figure S7a, a PG film was coated on a glass slide. Same areal mass density of 7.48 mg cm^{-2} was used. And surface temperature was -30 ºC with same ambient conditions. At first, PG film itself was free of frost, but it expanded and invaded into the frost zone (Figure S7b). Because PG's freezing point is much lower than water and they are miscible, PG can melt ice or frost when they encounter each other, resulting in PG/water solution. The advancement of PG front means the continuous dilution of PG. When the freezing point of the diluted solution reached the surface temperature, freezing occurred (Figure S7d), spread (Figure S7e), and at last covered all the film (Figure S7f).

In Figure S8a, PG drops were arrayed on a PDMS film since PG cannot spread over the film. To be mentioned, the CA of PG on the PDMS film is around 72º. Same areal mass density and

test conditions were applied. Frost quickly covered the PDMS film except the PG drop arrays (Figure S8b). Interestingly, there is a void between PG drops and the surrounding frost, which is due to the humidity sink effect of PG. The water vapor pressure profile around a PG drop with radius R is expressed as[21]

$$P(r) = P_\infty + (P_{PG} - P_\infty)R/r, \quad (4)$$

where r is the radial distance from the center of the PG drop, P_∞ is the water vapor pressure at infinity, and P_{PG} is the water vapor pressure above the PG drop. When $P(r)$ is larger than the water vapor saturation pressure at the surface (P_{SAT}), water vapor tends to condense on the surface. Therefore, the radius of the void (δ) is determined by

$$\frac{\delta}{R} = \frac{P_{PG} - P_\infty}{P_{SAT} - P_\infty}. \quad (5)$$

Considering the surface cooled to -30 ºC with air at 10 ºC and 42% relative humidity, P_∞ is 515.87 Pa, P_{SAT} is 50.94 Pa, and P_{PG} is ~ 6 Pa.[21,32] Then, $\delta/R \approx 1.09$, leading to a narrow region of inhibited condensation. If the surface temperature is lifted to -10 ºC, δ/R increases to 2.19. The frost thickness grew steadily, forming open frost domes around PG drops at some point,[21] which is indicated by the opaque PG drops (Figure S8d). Afterwards, PG drops were wicked into the frost and collapsed (Figure S8e).

The failure of PG film and drop arrays is observed to be accelerated by their contact with frost. On one hand, frost grows continuously, which prefers in the third direction if PG stands in its way on the surface. On the other hand, PG becomes dilute by absorbing ambient water vapor, accompanied by volume expansion and narrowing of region of inhibited condensation. For PG film, the latter plays a key role. And the former contributes large for PG drop arrays. Plots of frost coverage versus time for PG film, PG drop arrays, and PG-infused skeleton are shown in Figure S9. Though PG drop arrays take the longest time (165 min) to reach complete frosting, the frost coverage is more than 80% from the start. On the contrary, PG film maintains free of

frost up to 50 min, while frost covers all the film in 65 min. Here, PG-infused skeleton gets a good balance. At 50 min, its frost coverage is 10%, which is much lower than PG drop arrays. And its complete frosting time is about 140 min that is much longer than PG film.

EG, another glycol, was also infused into superhydrophobic skeleton. Its areal mass density is ~ 9.30 mg cm^{-2} mainly because of its smaller molecule size and lower viscosity than PG. And the frosting of EG-infused skeleton at -30 ºC with same ambient conditions is shown in Figure S10. Large condensed drops were observed and they resisted against freezing for a long time. Moreover, frost coverage versus time for EG-infused skeleton, compared with PG-infused skeleton, is plotted in Figure S11. Its anti-frosting performance is a little better than PG-infused skeleton because of its larger intake. To be emphasized, large condensed drops occurred on both glycol-infused skeletons whereas they are absent in PG film, PG drop arrays, superhydrophobic skeleton, and oil-infused skeleton. Raman spectra of condensed drops, water, and PG are shown in Figure 6a. Broad bands from 3000 to 3800 cm^{-1} are related to the OH stretching vibrations, the band around 2940 cm^{-1} is assigned to the stretching vibrations of CH_2 groups, the band around 1460 cm^{-1} is due to the deformation vibrations of CH_2 groups, and the band around 840 cm^{-1} is a marker of *gauche*-conformers of PG molecule.[33] No new peaks were found, so that condensed drops are composed of water and PG as expected.

Furthermore, Raman spectra of the condensed drops collected at different frosting time at -10 ºC were measured (Figure 6b). To be mentioned, after 200 min, some condensed drops got frozen, and all of them were iced in 360 min. Condensed drops were collected after melting if they had been frozen. It has been demonstrated that the intensity ratio of OH stretching band to CH_2 stretching band is a linear function of the molar ratio of water to PG.[33] In Figure 6b, the spectra are normalized to the peak intensity at 2936 cm^{-1}. Obviously, the intensity of OH

stretching band is increased with frosting time. Specifically, water/PG solutions with 10%, 50%, and 90% mol of PG were prepared and measured (Figure S12a). The peak intensity ratio (I_{3409}/I_{2936}) is linear to the molar ratio (C_{water}/C_{PG}) (Figure S12b). As noticed, the intercept is not zero because neat PG also has OH bonds. Using the linear fitting equation, the dependence of water: PG ratio on frosting time can be derived (Figure 6c). The concentration of PG in condensed drops is continuously diluted, leading to the gradually increased freezing point. From the water/PG phase diagram, the freezing point of -10 ºC roughly corresponds to V_{water}/V_{PG} of 3.5. Here, when condensed drops were all frozen, V_{water}/V_{PG} is larger than 4. This is because thick frost had grown along edges at 360 min.

Finally, the anti-frosting of PG-infused skeleton is schematically explained (Figure 6d-6f). First, the infused PG is underneath the surface asperities of the skeleton. When PG-infused skeleton is at -10 ºC and the air is at 10 ºC with 42% relative humidity, a water vapor pressure gradient is formed above the skeleton (Figure 6d). From equation (5), $\delta/R \approx 2.19$ at -10 ºC. Thus, the surface asperities are in the region of inhibited condensation due to the humidity sink effect of PG. Second, driven by the pressure gradient, PG-infused skeleton absorbs water vapor. Since the skeleton is hydrophobic, the absorbed water, mixed with PG, spills out of the skeleton, forming large condensed drops. Once the drops are generated, they are serving new humidity sinks (Figure 6e). Therefore, the condensed drops are continuing growing (Figure 6f), and the ratio of water in the condensed drops is fast increased (Figure 6c). This somehow mitigates the dilution of the PG in the skeleton, which will be further discussed in repeating test.

Anti-icing and de-icing performance

INT of water drops (10 μL) on superhydrophobic skeleton, oil-infused skeleton, and PG-infused skeleton was studied. And the results are -21.8 ± 1.7 ºC, -15.9 ± 1.5 ºC, and -33.9 ± 0.7

ºC, respectively (Figure 7a). It is worth noting that the anti-icing performance has a positive relationship with the anti-frosting performance because ice nucleation under condensation condition is correlated with condensation frosting,[9] which is elucidated in Figure 7b. A test water drop on a test surface is under cooling. Condensation emerges on the surface at certain temperature below the dew point that is determined by ambient conditions. Due to the low nucleation barrier, freezing occurs at the edges of the surface and propagates in a chain reaction to the center of the surface.[30] When attacked by the frost propagation, the test drop turns frozen. Therefore, the more early a close network of condensed drops forms, the higher INT is achieved. Since only sparse drops are condensed on PG-infused skeleton, ultra-low INT has been accomplished. Moreover, the test water drops before and after freezing are shown in Figure 7c-7e. The drops on superhydrophobic skeleton and oil-infused skeleton were observed to be surrounded by clusters of tiny condensed drops. And the water CA on superhydrophobic skeleton was substantially decreased due to the condensation-based impalement mechanism.[34,35] On the contrary, the large water CA on PG-infused skeleton was mostly retained because only sparse condensed drops were formed. And they did not freeze even at -40 ºC (Figure S13) owing to being doped with PG.

IAS was also tested. The data for superhydrophobic skeleton and oil-infused skeleton are 76.3 ± 6.2 and 28.4 ± 3.1 kPa, respectively. Same test procedures were tried for PG-infused skeleton, but it failed because water could not freeze on PG-infused skeleton at -10 ºC after 3 h. Therefore, ice cubes made in a fridge were transferred to the pre-cooled surface at -10 ºC. The surface was tilted by 25º. After 30 min, the ice cube could slide off the surface by its own gravity (Figure S14). The shear force (τ) has the form of

$$\tau = mg \sin \alpha, \quad (6)$$

where m is the mass of ice cube, g is the standard acceleration of gravity, and α is the tilting angle. Then, the IAS of PG-infused skeleton was calculated to be 41 Pa, which is three orders of magnitude smaller than those of superhydrophobic skeleton and oil-infused skeleton. The reason is PG can migrate to the ice cube by either spilling or bridging under vapor diffusion,[36] which then melts ice gradually. At some time, the generated interfacial liquid is enough to make the surface slippery. However, if PG is so diluted that the whole surface is frozen, the IAS surges to ~130 kPa.

Repeating and replenishing

Unlike antifreeze-imbibed hydrophilic surfaces that need replenishment every time after usage, the developed superhydrophobic skeleton infused with PG can be repeatably used, which is shown in Figure 8. In each frosting test, the temperature of PG-infused skeleton was controlled at -10 ºC, the ambient conditions were 42% of relative humidity and 10 ºC, and duration was 1 h. The infused mass before and after each test was measured (Figure 8a). And before weight measurement, the condensed drops on the surface were softly removed. With increasing the repeating number, the mass decreased continuously. No frost was guaranteed up to 10 repeating number (Figure 8b). At 11^{th} test, frost was formed in the middle of test. And frost was observed along the edges at the beginning of 12^{th} test. To be emphasized, the edges of samples is the most vulnerable part because they are near the surrounding frost (Figure 8e). Also, CAs and SAs were measured after each test (Figure S15). CAs were stable and SAs were slightly decreased with increasing repeating number, which hints that the depleted PG-infused skeleton is alike the superhydrophobic skeleton. Furthermore, replenishment of PG was implemented after 12^{th} test. Before that, the remained mass in the skeleton was fully expelled by putting samples at 40 ºC overnight. Same vacuum infiltration was applied, resulting in similar PG suction mass. And another 12 repeating tests were done. The results are shown in Figure 8a

and 8b. All can be repeated 10 times without frost, verifying good repeatable and replenishable abilities.

The condensed drops were further tested by Raman microscopy. As seen from Figure 9a, the peak ratio of I_{3409}/I_{2936} increases with repeat time. Accordingly, V_{water}/V_{PG} was calculated and the data are shown in Figure 9b. With increasing repeat time, V_{water}/V_{PG} increases fast. Furthermore, the remained liquid in PG-infused skeleton was measured during the repeat test. Here, the skeleton consists of ZnO and PDMS, which has characteristic peaks from 2800 to 3000 cm^{-1} (Figure 9c). They are owing to the stretching vibrations of CH_3 groups,[37] overlapping the peaks for CH_2 stretching vibrations. Therefore, the peak at 841 cm^{-1} was adopted because the peak ratio of I_{3409}/I_{841} is also a linear function of the molar ratio of water to PG.[33] Water/PG solutions with 10%, 50%, and 90% mol of PG were first tested and then the linear equation was attained (Figure S16). Afterwards, the PG-infused skeleton after test were detected. In Figure 9d, all spectra are normalized to the peak intensity at 841 cm^{-1}. Unexpectedly, the peak intensities at 3409 cm^{-1} just have a small change. The data of V_{water}/V_{PG} are shown in Figure 9b, verifying that the liquid in PG-infused skeleton after 1st test is a mixture of PG and water. More importantly, compared to the condensed drops, the dilution of PG inside the skeleton is much decelerated, highlighting the encaging effect of the superhydrophobic skeleton.

Performance comparison and application notes

In terms of anti-icing and anti-frosting, the superiority of PG-infused skeleton over superhydrophobic skeleton, oil-infused skeleton, PG film, and PG drop arrays is manifest. Here, it is further compared with some recent papers. Three classes of surfaces are selected, i.e., superhydrophobic surfaces, SLIPS, and antifreeze-based surfaces, whose details are listed in Table S1, S2, and S3, respectively. And the chosen data were all tested in a horizontal state.

Frankly, the comparison could not be rigorous because test conditions and procedures were different from paper to paper. Data of freezing delay time is shown in Figure 10a, which is an alternative index for INT. The longer the freezing delay time, the better the anti-icing performance. Same to the trend found here, SLIPS freeze first, then superhydrophobic surfaces, and the last is antifreeze-based surfaces. As for IAS comparison (Figure 10b), again antifreeze-based surfaces present the best performance. Averagely, SLIPS possess lower IAS than superhydrophobic surfaces. But it is hard to say for specific examples. The IAS could be as low as tens of Pa for antifreeze-based surfaces, which is two to four orders of magnitude lower than SLIPS or superhydrophobic surfaces. The last is anti-frosting property (Figure 10c). Complete frosting time is compared, which means the time needed for frosting all over the surface. As pointed out before, it is difficult to discern tiny condensates on superhydrophobic surfaces and SLIPS by bare eyes. Therefore, it is possible to overestimate them. As expected, anti-frosting performance of superhydrophobic surfaces and SLIPS is much worse than antifreeze-based surfaces.

There is no doubt that using antifreezes fundamentally enhances anti-icing and anti-frosting properties, which are conceivably related to the amounts of antifreezes. For a Boeing 727 airplane, 35 – 2000 mg cm^{-2} of PG is required.[17] As to antifreeze-based surfaces, different amounts were used, for example, 35 mg cm^{-2} for PG film and drop arrays[21], 208 mg cm^{-2} for PG-sucked nylon membrane covered by a superhydrophobic layer[25], 11.6 mg cm^{-2} for PG-sucked nylon membrane covered by a polycarbonate nanoporous membrane[26], and 104 mg cm^{-2} for PG-imbibed cotton textiles[17]. Though the least amount was used herein, superb anti-icing and anti-frosting performance is achieved, which showcases the advantages of exploiting the porous superhydrophobic skeleton to encage antifreezes. Although PG is generally considered environmentally friendly, it can have some negative impacts. Biodegradation is the significant

fate process of glycols in waters, which consumes oxygen. When glycols are in large amounts, a rapid depletion of the dissolved oxygen will occur, potentially harming aquatic life.[20] Also, PG is a commonly used solvent for pharmaceutical agent. However, its exposure to high dose for extended period may cause hyperosmolarity and metabolic acidosis.[38,39] Hence, PG of small amounts is preferred. Another concern is the method of adding PG. Opposite to the capillarity-driven self-infusion of oils into porous superhydrophobic skeletons,[40] vacuum infiltration is applied here. It may not be a bottleneck for large-scale application since vacuum infiltration method has been widely utilized in composite manufacturing industry.

Conclusions

Though PG cannot penetrate the superhydrophobic ZnO/PDMS porous skeleton through capillary action, it is vacuum-infiltrated into and stably resides in the skeleton. And the resulting PG-infused skeleton presents unexpected properties. The non-affinity between PG and the skeleton makes PG not cover the surface asperities, and thus the PG-infused skeleton inherits the superhydrophobicity from the skeleton. When in a humid and cooling condition, frost that promptly occurs on a conventional superhydrophobic surface is largely deferred on the PG-infused skeleton. Specifically, the PG-infused skeleton can delay the frost onset 6 times longer than the superhydrophobic skeleton. On one hand, due to the humidity sink effect of PG, the surface is in the region of inhibited condensation, avoiding the common tiny condensates. On the other hand, the absorbed water from the environment, mixed with PG, is spilled out of the skeleton, forming unique large and sparse condensed drops on the surface, which can keep non-frozen for an extra-long time. Moreover, the large condensed drops serve as new humidity sinks to delay the dilution of PG in the skeleton, and provide a slippery interfacial liquid to shed ice if any. Additionally, such self-secretion mitigates the volume expansion during freezing, leading to the durability under frosting/defrosting cycles. Despite not meeting three

principles for SLIPS,[41] the PG-infused skeleton possesses superhydrophobic and anti-icing/anti-frosting abilities simultaneously.

Supporting Information

Details of compared superhydrophobic surfaces (Table S1), SLIPS (Table S2), and antifreeze-based surfaces (Table S3) for comparison. Porosity and pore size distribution (Figure S1). Cross-sectional SEM images of superhydrophobic skeleton (Figure S2). FESEM image of superhydrophobic skeleton (Figure S3). Surface height profiles of superhydrophobic skeleton (Figure S4). Additional information about frosting of PG-infused skeleton at -10 ºC (Figure S5). Frost coverage versus frosting time (Figure S6, S9 and S11). Photos of frosting of PG film (Figure S7). Photos of frosting of PG drop arrays (Figure S8). Photos of frosting of EG-infused skeleton (Figure S10). Raman spectra of water/PG solutions (Figure S12 and S16). Additional information of icing test of PG-infused skeleton (Figure S13). De-icing photos (Figure S14). Change of wettability of PG-infused skeleton during repeating test (Figure S15).

Author Contributions

W.W. and M.N. conceived the idea for the work. M.N. guided the work. Sample fabrication was carried out by W.W. and Y.Y. Sample characterization was carried out by W.W. and Y.Y. Anti-frosting and anti-icing tests were carried out by W.W. and Y.Y. The manuscript was written by W.W and revised by W.W. and M.N. All authors helped shape the manuscript.

Acknowledgements

This work was supported by the Core Research for Evolutional Science and Technology (CREST) program “Revolution material development by fusion of strong experiments with

theory/data science" of the Japan Science and Technology Agency (JST), Japan, under Grant JPMJCR19J3.

References:

(1) Chen, F.; Wang, Y.; Tian, Y.; Zhang, D.; Song, J.; Crick, C. R.; Carmalt, C. J.; Parkin, I. P.; Lu, Y. Robust and Durable Liquid-Repellent Surfaces. *Chem. Soc. Rev.* **2022**, *51*, 8476–8583.

(2) Kreder, M. J.; Alvarenga, J.; Kim, P.; Aizenberg, J. Design of Anti-Icing Surfaces: Smooth, Textured or Slippery? *Nat. Rev. Mater.* **2016**, *1*, 15003.

(3) Lambley, H.; Schutzius, T. M.; Poulikakos, D. Superhydrophobic Surfaces for Extreme Environmental Conditions. *Proc. Natl. Acad. Sci. U. S. A.* **2020**, *117*, 27188–27194.

(4) Yin, L.; Wang, Y.; Ding, J.; Wang, Q.; Chen, Q. Water Condensation on Superhydrophobic Aluminum Surfaces with Different Low-Surface-Energy Coatings. *Appl. Surf. Sci.* **2012**, *258*, 4063–4068.

(5) Dhyani, A.; Wang, J.; Halvey, A. K.; Macdonald, B.; Mehta, G.; Tuteja, A. Design and Applications of Surfaces That Control the Accretion of Matter. *Science* **2021**, *373*, eaba5010.

(6) Boreyko, J. B.; Collier, C. P. Delayed Frost Growth on Jumping-Drop Superhydrophobic Surfaces. *ACS Nano* **2013**, *7*, 1618–1627.

(7) Chu, J.; Feng, X.; Li, Y.; Li, F.; Tian, G. Hierarchical Structure with Microcrater Covered with Nanograss Enhancing Condensation and Its Antifrosting/Anti-Icing Performance Inspired by Euphorbia Helioscopia L. *Langmuir* **2024**, *40*, 10313–10325.

(8) Di Novo, N. G.; Bagolini, A.; Pugno, N. M. Supercooled Condensation Droplets Sliding on Frost: Origin and Anti-Frosting Effect Observed on Cotinus Coggygria

Leaf. *iScience* **2024**, *27*, 111056.

(9) Weng, W.; Tenjimbayashi, M.; Naito, M. Role Variability of Surface Chemistry and Surface Topography in Anti-Icing Performance. *iScience* **2024**, *27*, 111039.

(10) Kim, P.; Wong, T. S.; Alvarenga, J.; Kreder, M. J.; Adorno-Martinez, W. E.; Aizenberg, J. Liquid-Infused Nanostructured Surfaces with Extreme Anti-Ice and Anti-Frost Performance. *ACS Nano* **2012**, *6*, 6569–6577.

(11) Haji, H. S.; Chang, T. H.; You, J. De; Chu, J. P.; Yiu, P. A Slippery and Icephobic Surface Based on Lubricant-Infused Metallic Glass Nanotube Array. *Appl. Surf. Sci.* **2025**, *690*, 162565.

(12) Song, X.; Hou, Y.; Zhang, X.; Zhao, Y.; Wu, Y.; Liu, M.; Guo, Z. Multiplex Biomimetic SLIPS With Super-Lubricity to Multiphase Matters. *Small* **2025**, *21*, 2407530.

(13) Anand, S.; Paxson, A. T.; Dhiman, R.; Smith, J. D.; Varanasi, K. K. Enhanced Condensation on Lubricant-Impregnated Nanotextured Surfaces. *ACS Nano* **2012**, *6*, 10122–10129.

(14) Zhao, H.; Ye, H.; Fazle Rabbi, K.; Wang, X.; Miljkovic, N.; Ho, J. Y. Micro- and Nanoengineered Metal Additively Manufactured Surfaces for Enhanced Anti-Frosting Applications. *ACS Appl. Mater. Interfaces* **2024**, *16*, 35697–35715.

(15) Guadarrama-Cetina, J.; Mongruel, A.; González-Viñas, W.; Beysens, D. Frost Formation with Salt. *EPL* **2015**, *110*, 56002.

(16) Liu, F.; Wang, Z.; Pan, Q. Intelligent Icephobic Surface toward Self-Deicing Capability. *ACS Sustain. Chem. Eng.* **2020**, *8*, 792–799.

(17) Yao, X.; Chen, B.; Morelle, X. P.; Suo, Z. Anti-Icing Propylene-Glycol Materials. *Extrem. Mech. Lett.* **2021**, *44*, 101225.

(18) Yoon, J.; Zhang, X.; Ryu, M.; Kim, W. H.; Ihm, K.; Lee, J. W.; Li, W.; Lee, H.

Tailoring the Hydrophilicity for Delayed Condensation Frosting in Antifogging Coatings. *ACS Appl. Mater. Interfaces* **2022**, *14*, 35064–35073.

(19) Deng, Q.; Wu, T.; Yin, K.; Li, X.; Wang, L.; Huang, Q.; Huang, Y.; Arnusch, C. J.; Duan, J. A. Efficient Anti-Frosting Enabled by Femtosecond Laser-Induced Salt-Philic and Superhydrophobic Surface. *Appl. Phys. Lett.* **2024**, *125*, 121602.

(20) Kent, R. A.; Andersen, D.; Caux, P. Y.; Teed, S. Canadian Water Quality Guidelines for Glycols - An Ecotoxicological Review of Glycols and Associated Aircraft Anti-Icing and Deicing Fluids. *Environ. Toxicol.* **1999**, *14*, 481–522.

(21) Sun, X.; Damle, V. G.; Uppal, A.; Linder, R.; Chandrashekar, S.; Mohan, A. R.; Rykaczewski, K. Inhibition of Condensation Frosting by Arrays of Hygroscopic Antifreeze Drops. *Langmuir* **2015**, *31*, 13743–13752.

(22) Lee, H.; Alcaraz, M. L.; Rubner, M. F.; Cohen, R. E. Zwitter-Wettability and Antifogging Coatings with Frost-Resisting Capabilities. *ACS Nano* **2013**, *7*, 2172–2185.

(23) Yamazaki, T.; Tenjimbayashi, M.; Manabe, K.; Moriya, T.; Nakamura, H.; Nakamura, T.; Matsubayashi, T.; Tsuge, Y.; Shiratori, S. Antifreeze Liquid-Infused Surface with High Transparency, Low Ice Adhesion Strength, and Antifrosting Properties Fabricated through a Spray Layer-by-Layer Method. *Ind. Eng. Chem. Res.* **2019**, *58*, 2225–2234.

(24) Wen, S. F.; Wang, Y. M.; Zhang, Z. M.; Liu, Y. L. Application of Anti-Icing Coating Based on Adsorption of Functional Substances by Microporous Sphere. *Prog. Org. Coatings* **2019**, *137*, 105320.

(25) Sun, X.; Damle, V. G.; Liu, S.; Rykaczewski, K. Bioinspired Stimuli-Responsive and Antifreeze-Secreting Anti-Icing Coatings. *Adv. Mater. Interfaces* **2015**, *2*, 1400479.

(26) Sun, X.; Rykaczewski, K. Suppression of Frost Nucleation Achieved Using the

Nanoengineered Integral Humidity Sink Effect. *ACS Nano* **2017**, *11*, 906–917.

(27) Yamauchi, Y.; Tenjimbayashi, M.; Samitsu, S.; Naito, M. Durable and Flexible Superhydrophobic Materials: Abrasion/Scratching/Slicing/Droplet Impacting/Bending/Twisting-Tolerant Composite with Porcupinefish-like Structure. *ACS Appl. Mater. Interfaces* **2019**, *11*, 32381–32389.

(28) Daniel, D.; Timonen, J. V. I.; Li, R.; Velling, S. J.; Kreder, M. J.; Tetreault, A.; Aizenberg, J. Origins of Extreme Liquid Repellency on Structured, Flat, and Lubricated Hydrophobic Surfaces. *Phys. Rev. Lett.* **2018**, *120*, 244503.

(29) Jung, Y. C.; Bhushan, B. Dynamic Effects of Bouncing Water Droplets on Superhydrophobic Surfaces. *Langmuir* **2008**, *24*, 6262–6269.

(30) Yang, S.; Wu, C.; Zhao, G.; Sun, J.; Yao, X.; Ma, X.; Wang, Z. Condensation Frosting and Passive Anti-Frosting. *Cell Reports Phys. Sci.* **2021**, *2*, 100474.

(31) Hauer, L.; Wong, W. S. Y.; Donadei, V.; Hegner, K. I.; Kondic, L.; Vollmer, D. How Frost Forms and Grows on Lubricated Micro- And Nanostructured Surfaces. *ACS Nano* **2021**, *15*, 4658–4668.

(32) Nath, S.; Boreyko, J. B. On Localized Vapor Pressure Gradients Governing Condensation and Frost Phenomena. *Langmuir* **2016**, *32*, 8350–8365.

(33) Liubimovskii, S. O.; Novikov, V. S.; Ustynyuk, L. Y.; Ivchenko, P. V.; Prokhorov, K. A.; Kuzmin, V. V.; Sagitova, E. A.; Godyaeva, M. M.; Gudkov, S. V.; Darvin, M. E.; Nikolaeva, G. Y. Raman Structural Study of Ethylene Glycol and 1,3-Propylene Glycol Aqueous Solutions. *Spectrochim. Acta - Part A Mol. Biomol. Spectrosc.* **2023**, *285*, 121927.

(34) Weng, W.; Zheng, X.; Tenjimbayashi, M.; Watanabe, I.; Naito, M. De-Icing Performance Evolution with Increasing Hydrophobicity by Regulating Surface Topography. *Sci. Technol. Adv. Mater.* **2024**, *25*, 2334199.

(35) Wang, L.; Tian, Z.; Jiang, G.; Luo, X.; Chen, C.; Hu, X.; Zhang, H.; Zhong, M. Spontaneous Dewetting Transitions of Droplets during Icing & Melting Cycle. *Nat. Commun.* **2022**, *13*, 378.

(36) Chavan, S.; Park, D.; Singla, N.; Sokalski, P.; Boyina, K.; Miljkovic, N. Effect of Latent Heat Released by Freezing Droplets during Frost Wave Propagation. *Langmuir* **2018**, *34*, 6636–6644.

(37) Cai, D.; Neyer, A.; Kuckuk, R.; Heise, H. M. Raman, Mid-Infrared, near-Infrared and Ultraviolet-Visible Spectroscopy of PDMS Silicone Rubber for Characterization of Polymer Optical Waveguide Materials. *J. Mol. Struct.* **2010**, *976*, 274–281.

(38) Zar, T.; Graeber, C.; Perazella, M. A. Recognition, Treatment, and Prevention of Propylene Glycol Toxicity. *Semin. Dial.* **2007**, *20*, 217–219.

(39) Bhattarai, B. C.; Parajuli, A. Evaluating the Effectiveness of Propylene Glycol and Ethanol as Antifreeze : An Environmentally Friendly Alternative. *Front. Environ. Eng.* **2025**, *3*, 1519115.

(40) Misra, S.; Tenjimbayashi, M.; Weng, W.; Mitra, S. K.; Naito, M. Bioinspired Scalable Lubricated Bicontinuous Porous Composites with Self-Recoverability and Exceptional Outdoor Durability. *ACS Appl. Mater. Interfaces* **2023**, *15*, 36839–36855.

(41) Wong, T. S.; Kang, S. H.; Tang, S. K. Y.; Smythe, E. J.; Hatton, B. D.; Grinthal, A.; Aizenberg, J. Bioinspired Self-Repairing Slippery Surfaces with Pressure-Stable Omniphobicity. *Nature* **2011**, *477*, 443–447.

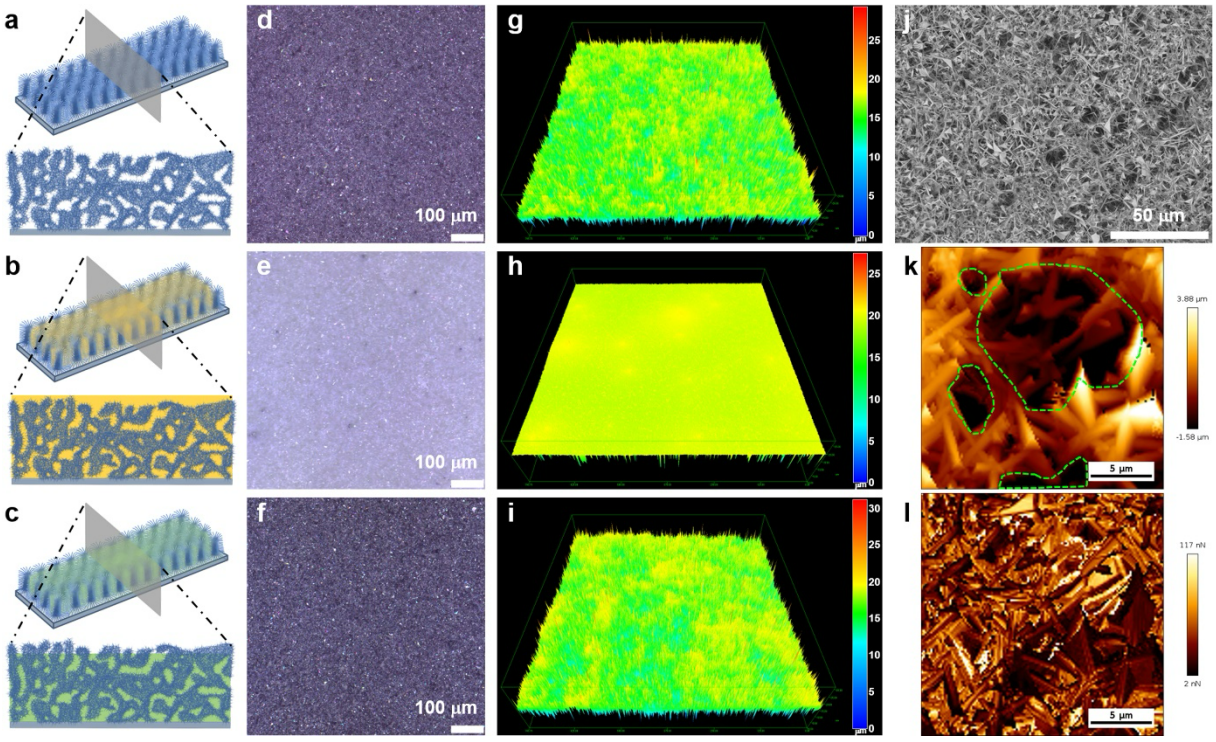

Figure 1. Schematics of a) superhydrophobic skeleton, b) silicone oil-infused skeleton, and c) PG-infused skeleton. Top-view images of d) superhydrophobic skeleton, e) silicone oil-infused skeleton, and f) PG-infused skeleton by laser scanning confocal microscopy. 3D images of g) superhydrophobic skeleton, h) silicone oil-infused skeleton, and i) PG-infused skeleton by laser scanning confocal microscopy. Test areas are 750 µm × 750 µm. j) SEM image of superhydrophobic skeleton. AFM images of PG-infused skeleton with k) height mode and l) adhesion mode.

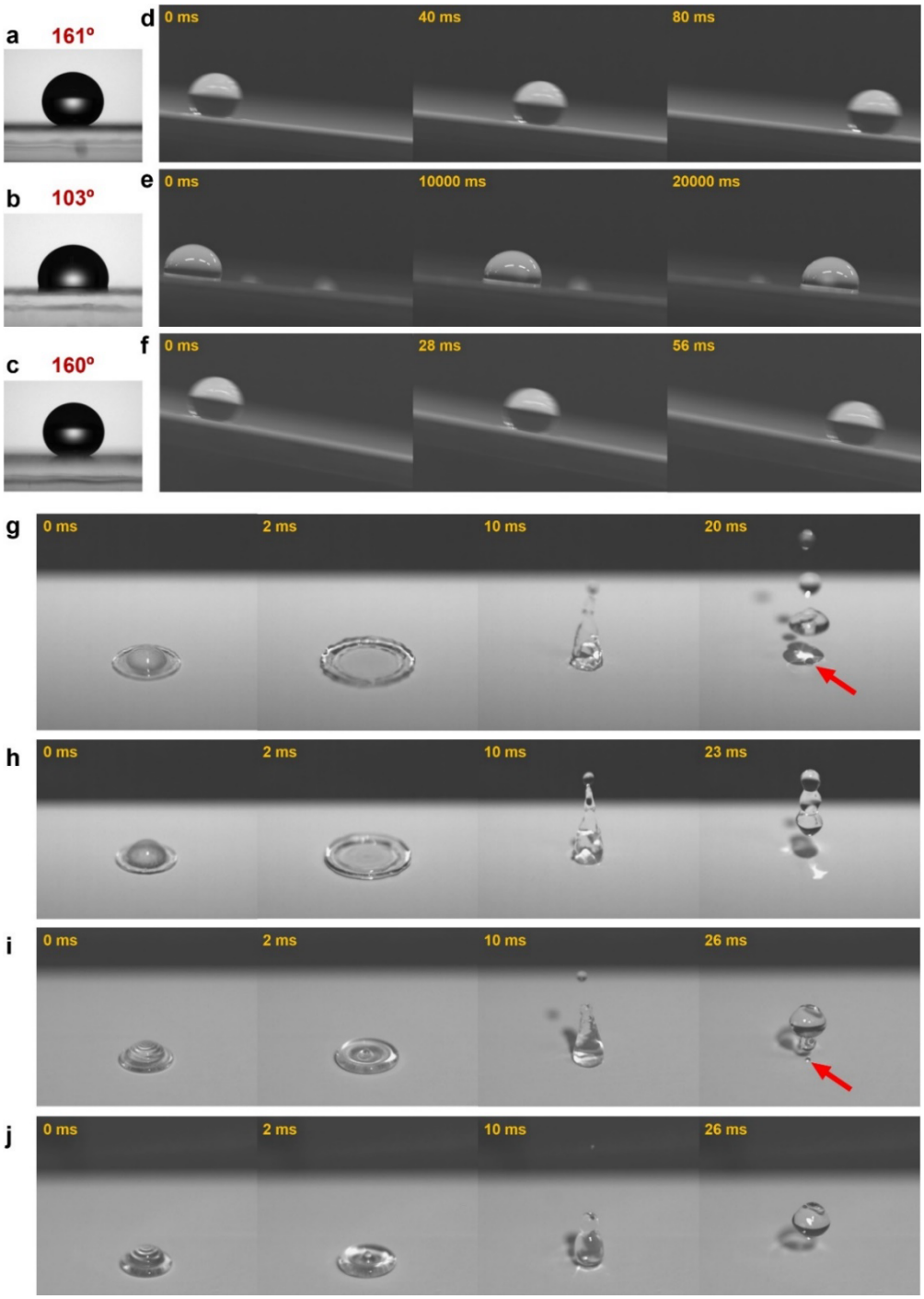

Figure 2. Water drops sitting on a) superhydrophobic skeleton, b) silicone oil-infused skeleton, and c) PG-infused skeleton. Water drops sliding on d) superhydrophobic skeleton (tilted 5º), e) silicone oil-infused skeleton (tilted 5º), and f) PG-infused skeleton (tilted 10º). Water drop impacting on superhydrophobic skeleton with velocities of g) 1.40 m s^{-1} and h) 1.25 m s^{-1}. Water drop impacting on PG-infused skeleton with velocities of i) 0.77 m s^{-1} and j) 0.63 m s^{-1}.

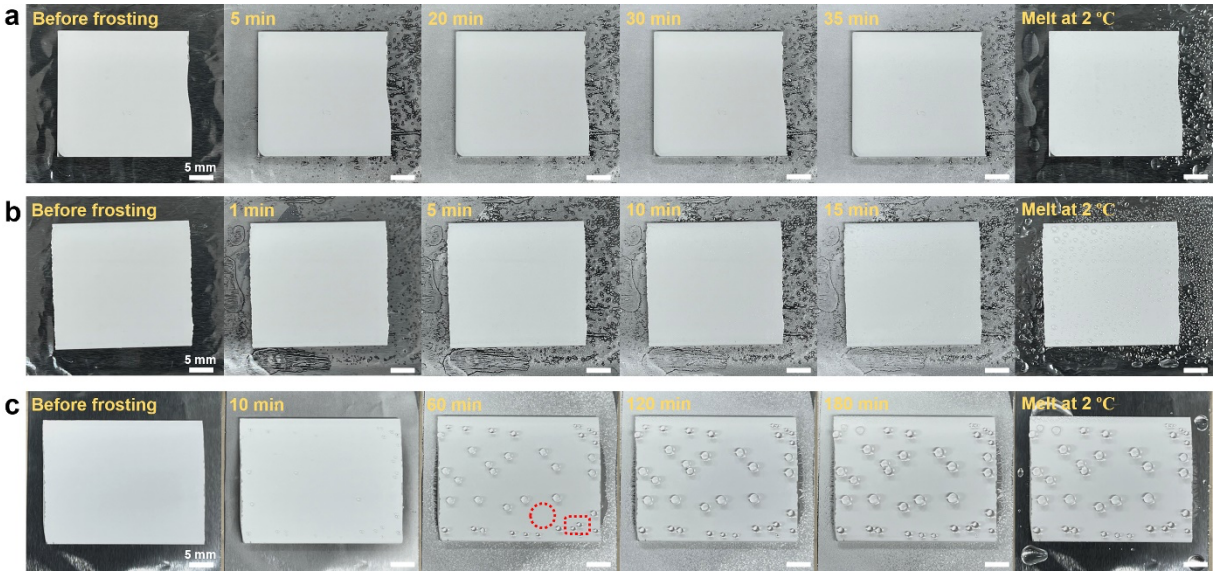

Figure 3. Photos of evolution of a) superhydrophobic skeleton, b) silicone oil-infused skeleton, and c) PG-infused skeleton at -10 ºC with ambient conditions of 42% of relative humidity and 10 ºC. All samples were horizontally placed.

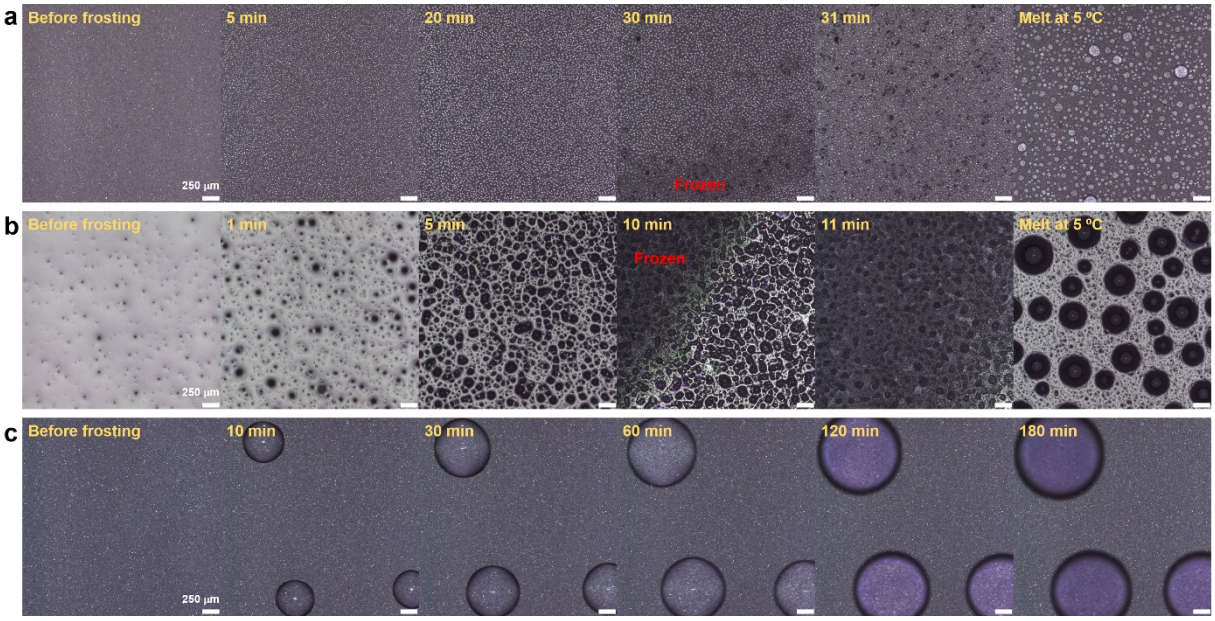

Figure 4. Images of evolution of a) superhydrophobic skeleton, b) silicone oil-infused skeleton, and c) PG-infused skeleton at -10 ºC with ambient conditions of 42% of relative humidity and 10 ºC by laser scanning confocal microscopy. All samples were horizontally placed.

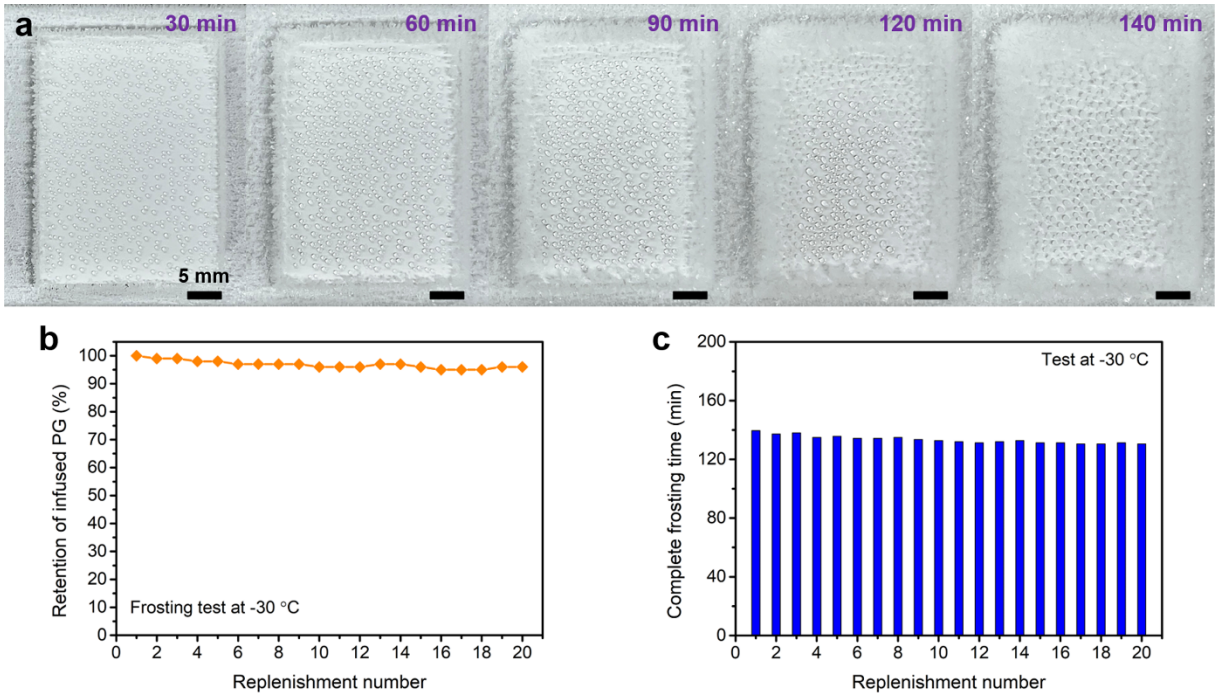

Figure 5. Frosting/defrosting/replenishing test of PG-infused skeleton at -30 ºC with ambient conditions of 42% of relative humidity and 10 ºC. a) Evolution of PG-infused skeleton with time. b) Change of infused PG mass with replenishment number. c) Change of complete frosting time with replenishment number.

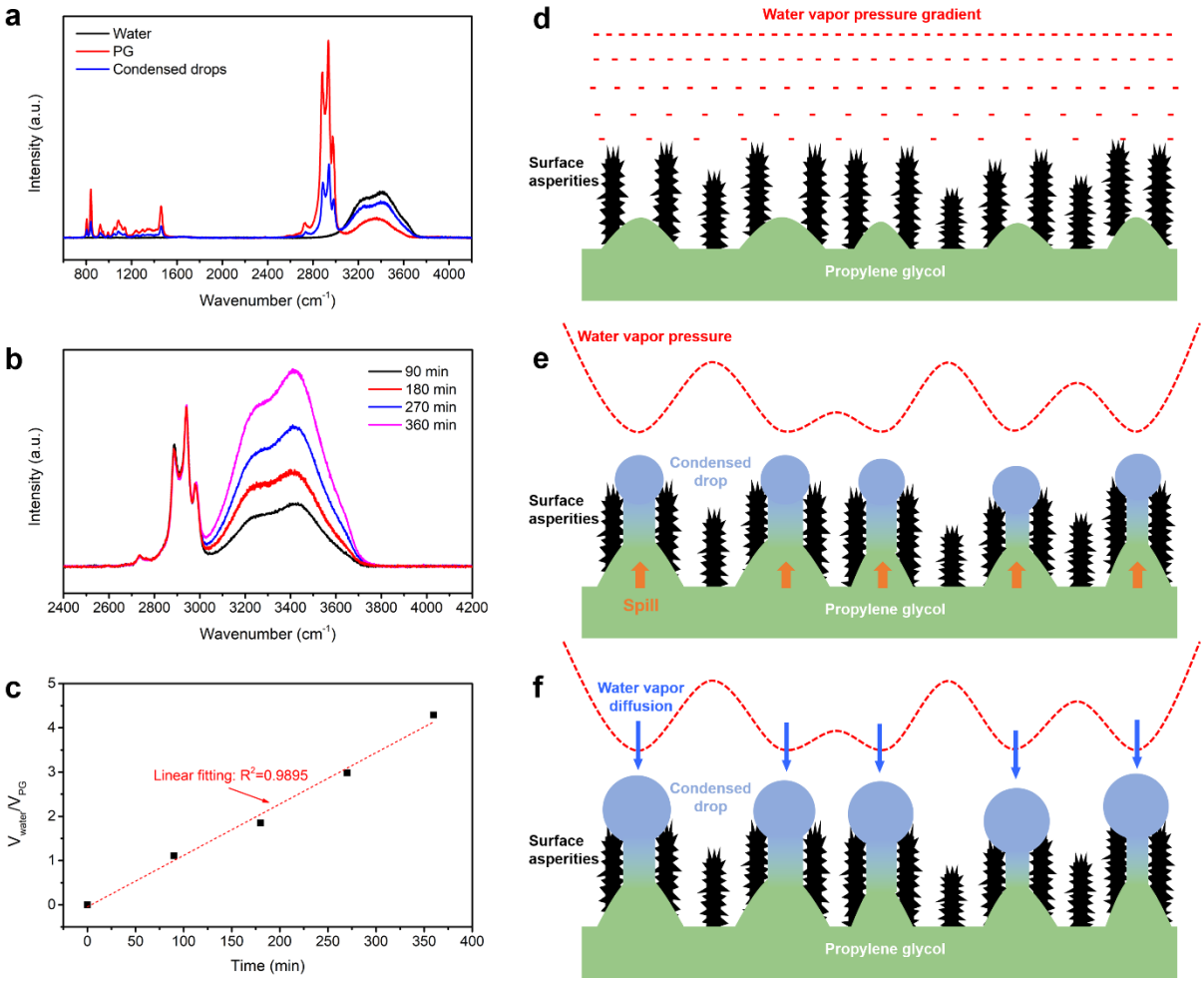

Figure 6. a) Raman spectra of water, PG, and condensed drops on PG-infused skeleton under cooling. b) Dependence of Raman spectra of condensed drops on frosting time. c) Dependence of volume ratio of water to PG for condensed drops on frosting time. d-f) Schematics of evolution of PG-infused skeleton being cooled in a humid environment. d) Water vapor pressure gradient above PG-infused skeleton at the start. e) Formation of condensed drops on the surface and reconstruction of water vapor pressure gradient above the skeleton after some time. f) Continuous growth of the condensed drops until freezing.

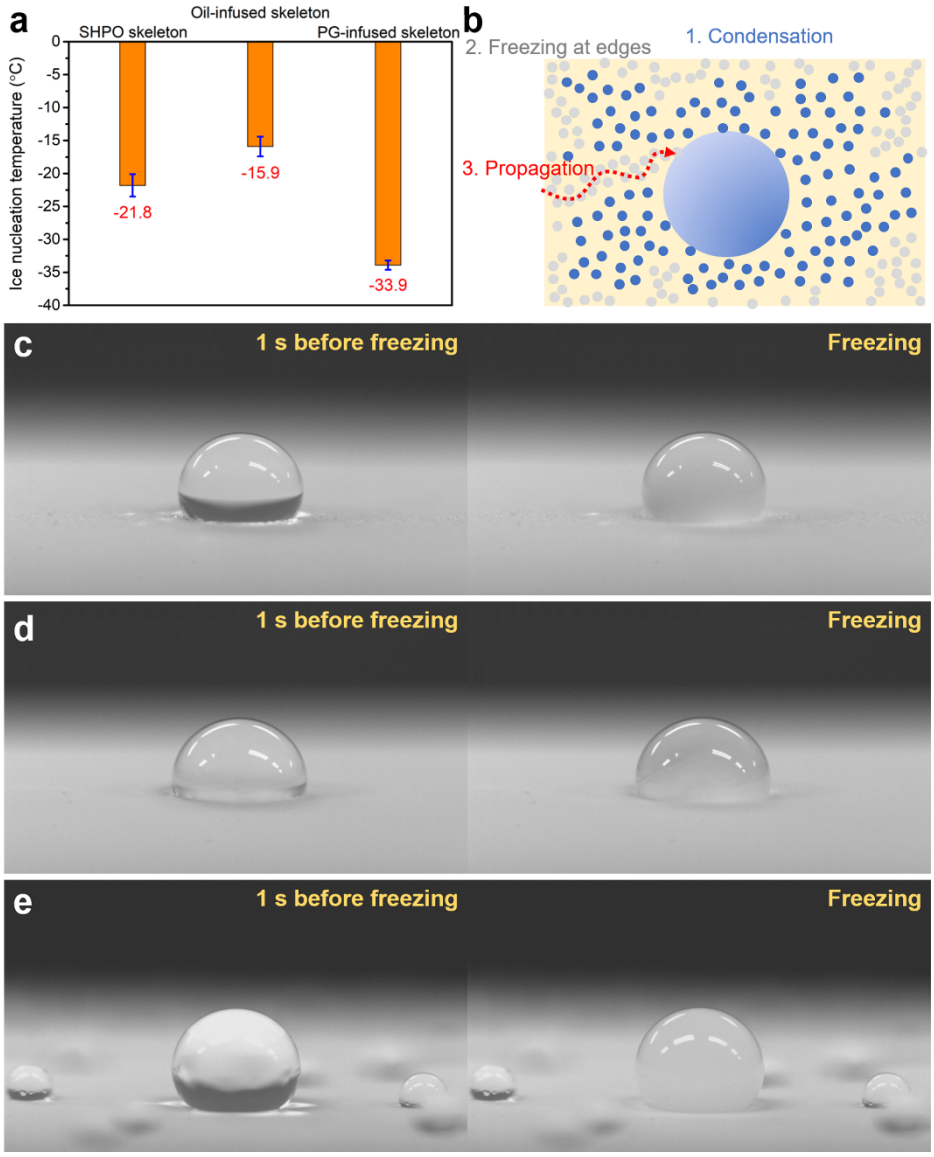

Figure 7. a) INT data for superhydrophobic (SHPO) skeleton, silicone oil-infused skeleton, and PG-infused skeleton. b) Illustration of ice nucleation mechanism with the existence of condensation and frosting. Photos of water drops before and after freezing on c) superhydrophobic skeleton, d) silicone oil-infused skeleton, and e) PG-infused skeleton.

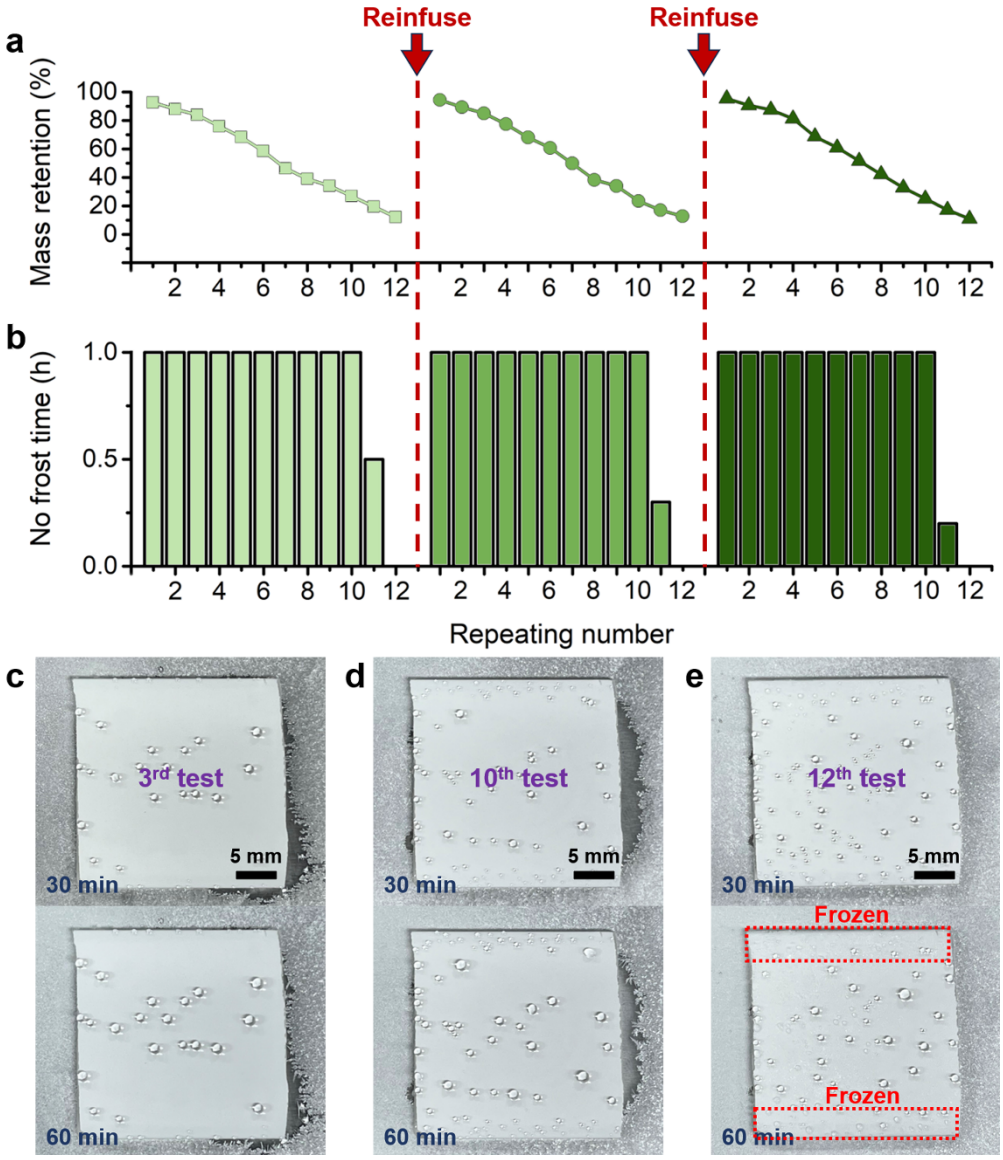

Figure 8. Repeating and replenishing tests of PG-infused skeleton at -10 ºC with ambient conditions of 42% of relative humidity and 10 ºC. a) Change of infused mass with repeating time. b) Change of no frost time with repeating time. Photos of PG-infused skeleton during c) 3rd test, d) 10th test, and e) 12th test in the first batch.

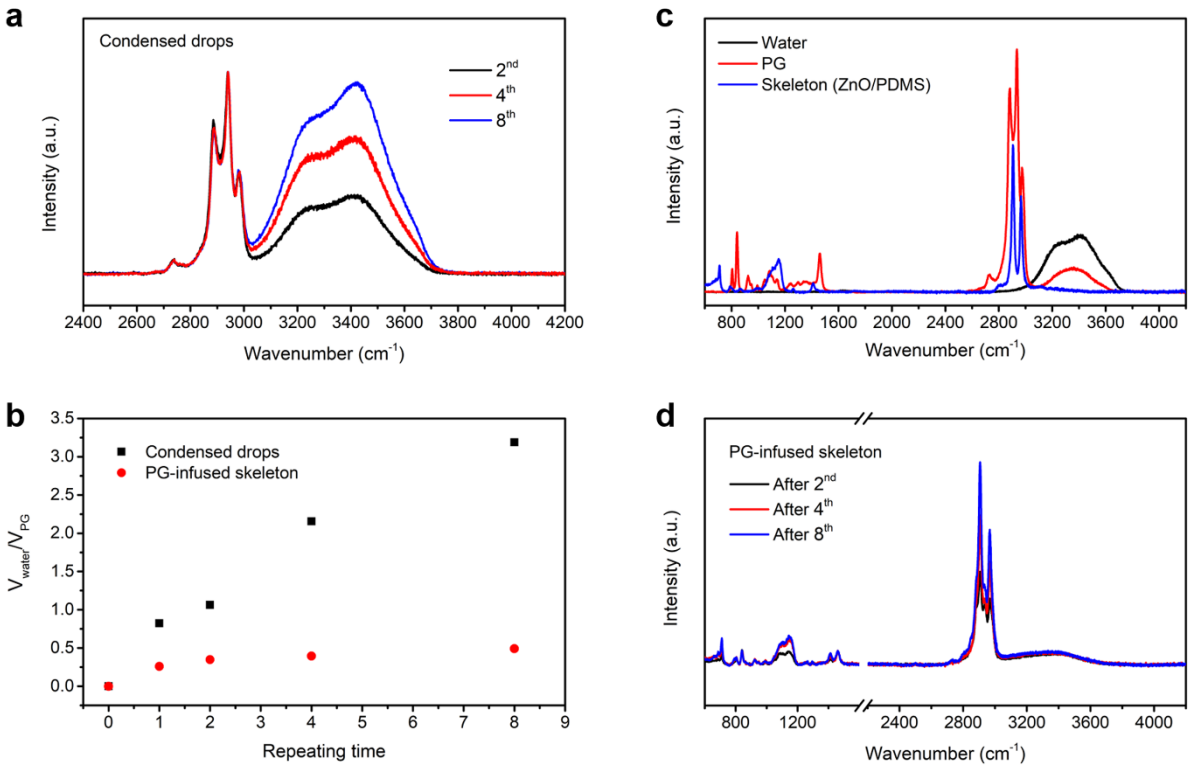

Figure 9. a) Raman spectra of condensed drops on PG-infused skeleton under cooling in repeating test. b) Dependence of volume ratio of water to PG for condensed drops and liquid remained inside PG-infused skeleton on repeating time. c) Raman spectra of water, PG, and skeleton. d) Dependence of Raman spectra of PG-infused skeleton on repeating time.

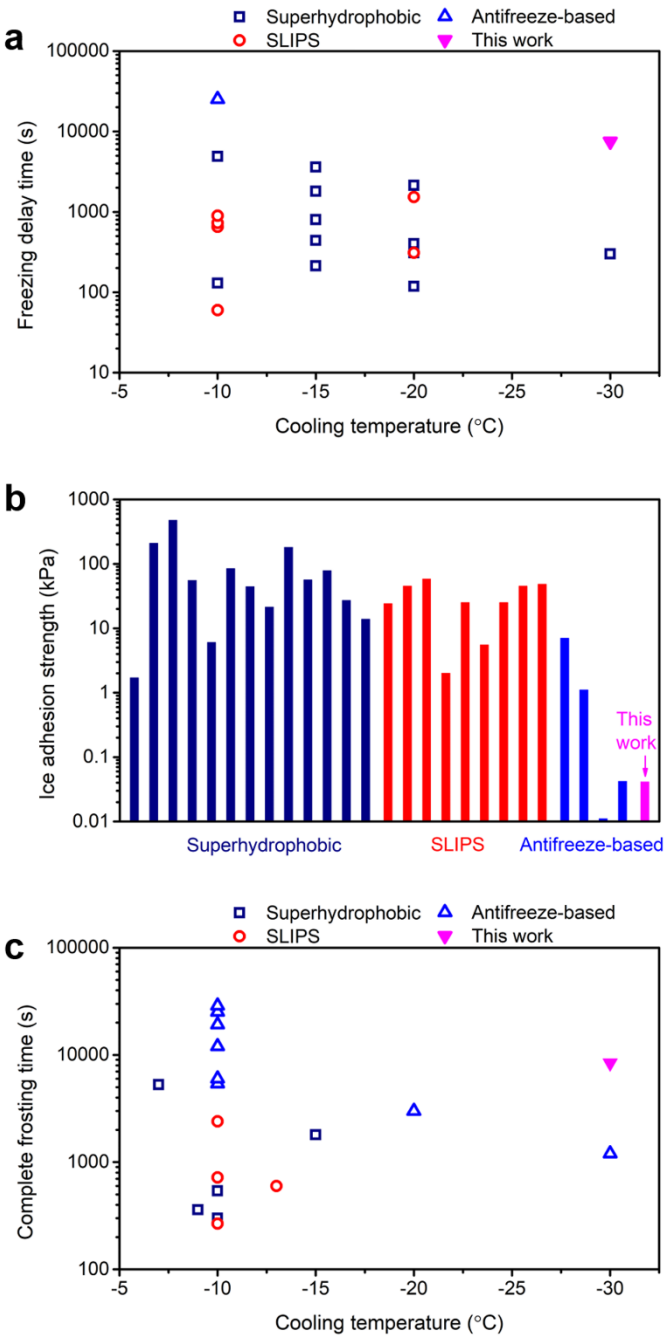

Figure 10. Comparison between PG-infused skeleton (this work) and some reported superhydrophobic surfaces, SLIPS, and antifreeze-based surfaces in a) freezing delay time, b) IAS, and c) complete frosting time.

TOC Graphic

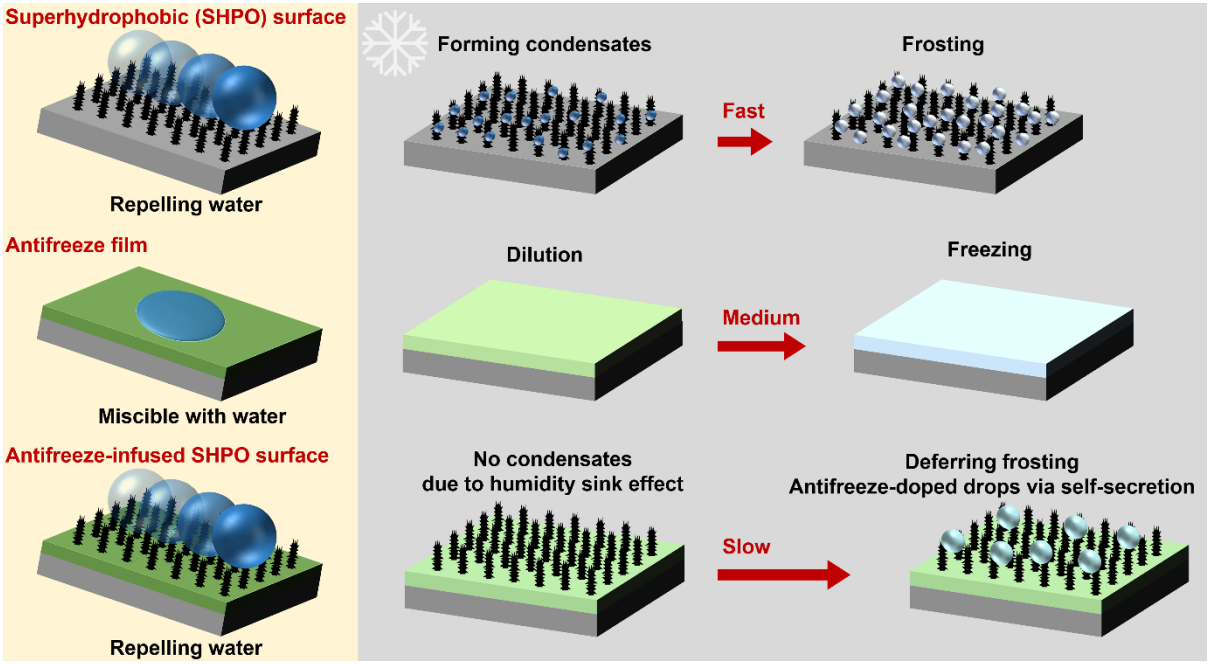
Superhydrophobic (SHPO) surface
Repelling water
Antifreeze film
Miscible with water
Antifreeze-infused SHPO surface
Repelling water
Forming condensates
Frosting
Fast
Dilution
Freezing
Medium
No condensates
due to humidity sink effect
Deferring frosting
Antifreeze-doped drops via self-secretion
Slow